The effect of *Drosophila attP40* background on the glomerular organization of Or47b olfactory receptor neurons

Qichen Duan, Rachel Estrella, Allison Carson, Yang Chen (iD), Pelin C. Volkan (iD)*

Department of Biology, Duke University, Durham, NC 27708, USA

*Corresponding author: Volkan Lab, Room 4341, French Family Science Center, 124 Science Drive, Campus Box 90338, Duke University, Durham, NC 27708.
Email: pelin.volkan@duke.edu

Abstract

Bacteriophage integrase-directed insertion of transgenic constructs into specific genomic loci has been widely used by *Drosophila* community. The *attP40* landing site located on the second chromosome gained popularity because of its high inducible transgene expression levels. Here, unexpectedly, we found that homozygous *attP40* chromosome disrupts normal glomerular organization of Or47b olfactory receptor neuron (ORN) class in *Drosophila*. This effect is not likely to be caused by the loss of function of *Msp300*, where the *attP40* docking site is inserted. Moreover, the *attP40* background seems to genetically interact with the second chromosome *Or47b-GAL4* driver, which results in a similar glomerular defect. Whether the ORN phenotype is caused by the neighbouring genes around *Msp300* locus in the presence of *attP40*-based insertions or a second unknown mutation in the *attP40* background remains elusive. Our findings tell a cautionary tale about using this popular transgenic landing site, highlighting the importance of rigorous controls to rule out the *attP40* landing site-associated background effects.

Keywords: *Drosophila*, *attP40*, olfactory receptor neuron, axon terminal organization

Introduction

RNA interference (RNAi)-based genetic screens provide scientists with powerful tools to identify genes involved in various biological processes (Housden *et al.* 2017). Binary expression systems, such as the *GAL4/UAS* system, induce the expression of various effectors in the desired cell populations (Brand and Perrimon 1993). In Drosophila carrying transgenes for both cell-type-specific promoter-driven *GAL4* (driver) and *UAS-RNAi*, GAL4 protein binds *UAS* sites and drives *RNAi* expression, disrupting the expression and function of the target gene (Brand and Perrimon 1993). As RNAi-based knockdown methods were becoming popular, efforts were initiated to make transgenic libraries of flies carrying *UAS-RNAi* targeting all the genes in the genome (Dietzl *et al.* 2007; Ni *et al.* 2009, 2011; Perkins *et al.* 2015). These genome-wide libraries were then followed by efforts to generate thousands of *GAL4* lines that restrict expression to cellular subpopulations, enabling loss-of-function screens in cells of interest.

Among the RNAi collections, stocks from Transgenic RNAi Project (TRiP) have gained popularity because of their targeted integration of *UAS-RNAi* transgenes into the genome, efficient expression induced by appropriate *GAL4* drivers in different tissues, and high specificity with minimal expected off-target effects (Markstein *et al.* 2008; Ni *et al.* 2008; Perkins *et al.* 2015). To expedite the generation of transgenic libraries, two predetermined chromosomal docking sites were targeted for recombination

events that insert *UAS-RNAi* transgenes: *attP40* on the second chromosome and *attP2* on the third chromosome (Markstein *et al.* 2008). With the presence of bacteriophage-originated phiC31 integrase (by co-injection of integrase mRNA or germline-expressing transgenic integrase), the *UAS-RNAi* construct can be inserted into the corresponding docking sites (Groth *et al.* 2004; Ni *et al.* 2008). These two sites, *attP40* and *attP2*, are selected because they exhibit optimal inducible expression levels upon binding with diverse tissue-specific *GAL4* drivers (Markstein *et al.* 2008). Therefore, in addition to the TRiP *UAS-RNAi* library, many other transgenes, including tissue-specific drivers (*GAL4*, *QF*, *LexA*) and *UAS/QUAS/LexAop-effectors/reporters* are also routinely integrated into these two landing sites (Zirin *et al.* 2020).

Given the widespread use of transgenic flies with *attP40* and *attP2* backbones, and the lesson learned from another popular *UAS-RNAi* collection with reported non-specific effects due to transgenic docking sites (Green *et al.* 2014; Vissers *et al.* 2016), we must be more cognizant of potential phenotypic influences from these genetic backgrounds. Both *attP40* and *attP2* docking sites are in chromosomal regions populated by many genes. These sites, like any insertion into the genome, can disrupt function of nearby genes. More specifically, the *attP40* site is located within one of the large introns of *Msp300* gene while *attP2* site is inserted in the 5′ untranslated region (UTR) of *Mocs1* gene (Larkin *et al.* 2020). Both Msp300 and Mocs1 have critical biological roles.

Specifically, Msp300 is the *Drosophila melanogaster* orthologue of mammalian Nesprins, which organize postsynaptic cytoskeleton scaffold and are required for stabilization of new synapses (Elhanany-Tamir *et al.* 2012; Morel *et al.* 2014; Titlow *et al.* 2020; Zheng *et al.* 2020). Mocs1 is involved in Mo-molybdopterin cofactor biosynthetic process and inter-male aggressive behaviours (Gaudet *et al.* 2011; Ramin *et al.* 2019). It is unclear how the insertion of various transgenic constructs into *attP40* and *attP2* docking sites would affect the function of these host genes which may further result in phenotypic defects.

Indeed, recent studies have raised issues related to landing site-associated effects. For example, van der Graaf *et al.* 2022 showed flies bearing two copies of *attP40*-derived insertions also show decreased *Msp300* transcript levels (van der Graaf *et al.* 2022). In addition, this study also reported defects in muscle nuclei spacing in larval stages in the *attP40* homozygous background, which phenocopies *Msp300* mutants (van der Graaf *et al.* 2022). These results suggest that the *attP40* docking site and *attP40*-based transgenes are insertional mutations of *Msp300* gene (van der Graaf *et al.* 2022). Another study reported that *attP40* flies show resistance to cisplatin-induced neuronal damage, compared to the *attP2* background (Groen *et al.* 2022). This study tied the effect to the reduced *ND-13A* (NADH dehydrogenase 13 kDA subunit, a component of mitochondrial complex I) expression in *attP40* homozygous flies (Groen *et al.* 2022). It is noteworthy that *ND-13A* flanks the 5′ UTR of *Msp300* and is downstream of *attP40* docking site. Together, these results imply the integration of *attP40* docking site significantly changes the local transcriptional state and interferes with the transcription of surrounding genes.

During a GAL4-driven *UAS-RNAi* screen for olfactory neuron axon organization, we observed an axon terminal phenotype that is associated with the *attP40* background. The phenotype occurs in the flies homozygous for the *attP40* docking site alone or with various transgenic insertions, independent of the identity of the transgene. Notably, the phenotype observed in the *attP40* background appears to be recessive but is independent of the *Msp300* function, possibly implicating other *attP40* background mutations nearby or in other locations on the second chromosome. Though the nature of the mutation is unclear, the background effects should be mitigated by designing more rigorous controls to interpret phenotypic data obtained using reagents in concert with the *attP40* background.

Materials and methods

Drosophila stocks and genetics

Drosophila were raised in classic molasses media provided by Archon Scientific. For the RNAi screen experiments, flies were raised at 28°C to maximize the knockdown efficiency. Most of the other crosses were also kept at 28°C, except for the experiments shown in Figs. 1, f and g and 3a, which were conducted at room temperature (23°C). After eclosion, the flies are aged for 5–7 days before dissection. In addition to the *UAS-RNAi* stocks from Bloomington Drosophila Stock Center (listed in Fig. 1b), the following stocks are used: *UAS-RFP RNAi attP2* (BDSC# 35785), *UAS-beat-Ia RNAi #3 GD1386* (VDRC# 4544), *UAS-SMC3 RNAi attP2* (BDSC# 60017), *UAS-SMC3 RNAi attP40* (BDSC# 50899), *UAS-vtd RNAi attP2* (BDSC# 36786), *UAS-vtd RNAi attP40* (BDSC# 65229), *attP40* (BDSC# 36304), *attP2* (BDSC# 36303), *ctrl-gRNA attP40* (BDSC# 67539), *UAS-RFP attP40* (BDSC# 32222), *UAS-rCD2.RFP attP2* (BDSC# 56179), *UAS-rCD2.RFP attP5* (BDSC# 56180), *UAS-rCD2.RFP attP40* (BDSC# 56181), *Msp300^{AKASH}* (BDSC# 26781),

Msp300^{MI01145} (BDSC# 53050), *Msp300^{MI00111}* (BDSC# 30623), *Msp300^{KG03631}* (BDSC# 13024); *Or47b-GAL4* (chr2, BDSC#9983), *Or47b-GAL4* (chr3, BDSC#9984), *Or43a-GAL4* (chr2), *Or47a-GAL4* (chr2) (Vosshall *et al.* 2000; Fishilevich and Vosshall 2005), and *Gr21a-GAL4* (chr2) (Scott *et al.* 2001) are gifts from Dr. Leslie Vosshall; *UAS-Syt.GFP* (chr2 or chr3), *UAS-mCD8.GFP, UAS-RFP* are Volkan lab stocks (Barish *et al.* 2018). The line *Or47b-GAL4, Or47a-GAL4, Or43a-GAL4, Gr21a-GAL4, UAS-Syt.GFP/CyO* (short for *4xOr-GAL4 > Syt.GFP*) was recombined and balanced from the above components.

Immunocytochemistry

Flies were sacrificed in 70% ethanol. Fly brains were then dissected in PBST buffer (0.2% Triton X-100 in 1X PBS), fixed in 4% paraformaldehyde for 30 min, followed by washing with PBST for three 10-min cycles. Brains were incubated in the primary antibody mix at 4°C overnight, followed by three 20-min washes with PBST at room temperature, then incubated in the secondary antibody mix at 4°C overnight. The brains were washed again by three 20-min wash with PBST before being mounted on the slide for imaging. The blocking was done together with each antibody incubation, with 1% natural goat serum mixed with primary and secondary antibodies, respectively. The following primary antibodies were used: 1:1000 rabbit anti-GFP (Invitrogen), 1:20 rat anti-Ncad (DSHB); the following secondary antibodies were used: 1:1000 Alexa Fluor 488 goat anti-rabbit IgG (Invitrogen), 1:200 Alexa Fluor 647 goat anti-rat IgG (Invitrogen); all antibodies are diluted in PBST.

Confocal imaging and phenotypic quantification

Confocal imaging was performed by either Olympus Fluoview FV1000 microscope or Zeiss 880 microscope. Brains were imaged across Z-axis from the posterior side to the most anterior side of the antennal lobes, and all confocal sections were overlaid for phenotypical analysis. The same set of imaging parameters was used between experimental and control groups. The phenotype was qualitatively determined by glomerular morphology, i.e. whether Or47b ORN axons appear in the dorsal antennal lobe region, in contrast to the typical V-shaped glomerulus in wild-type controls. The phenotype shown in Fig. 1 (glomerular expansion) is largely consistent from brain to brain, while the phenotypes shown in Fig. 2, b and e exhibit variability, which were categorized into expansion or dorsal shift. The phenotype was quantified by the percentage of antennal lobes exhibiting each defect among all the brains examined in respective groups. *P*-value was calculated by two-tailed Fisher's exact test through the built-in functions of GraphPad Prism 9 software.

Inverse PCR to recover the genomic DNA sequence flanking the *Or47b-GAL4* transgenic insertion

Or47b-GAL4 transgene was inserted into an unknown region on the second chromosome by P-element-mediated method (Vosshall *et al.* 2000). The P-element structure of *Or47b-GAL4* transgene was shown in the Fig. 3b. We used previously described inverse PCR method (Huang *et al.* 2009) to identify the genomic sequence flanking the insertion site. Briefly, genomic DNA was first extracted from 30 *Or47b-GAL4* flies (BDSC# 9983), followed by overnight digestion with any of three restriction enzymes, MspI, HinP1I, or Sau3AI (New England BioLabs). Each digest was then ligated by T4 DNA ligase (New England BioLabs) in larger volume (400 µl, see (Huang *et al.* 2009) for mix details) to promote intramolecular ligation while minimizing intermolecular ligation. Ligation was performed at 16°C overnight. The unknown flanking
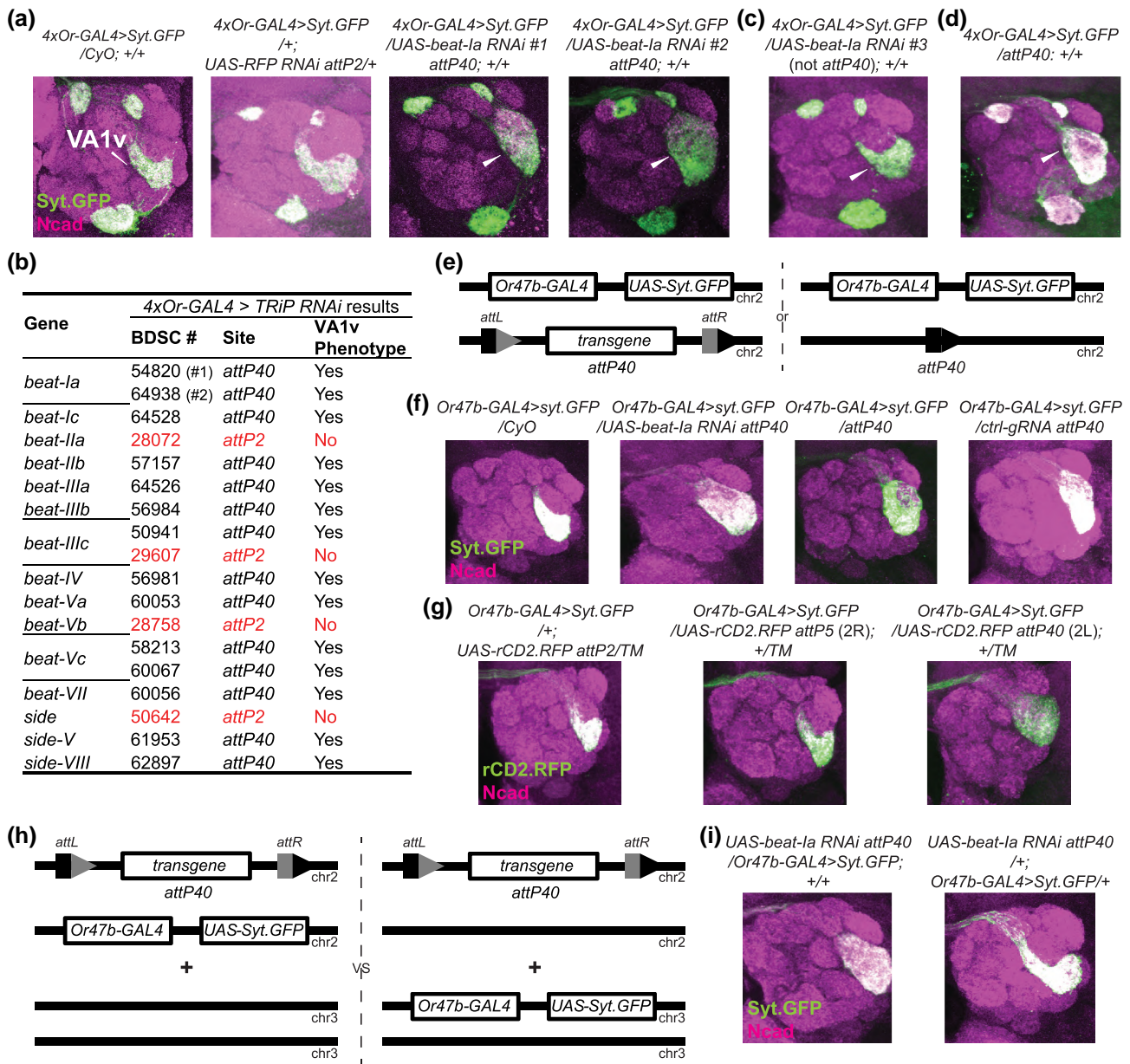
Fig. 1. Genetic interactions between *attP40* and *Or47b-GAL4* backgrounds on the second chromosome disrupt the glomerular organization of Or47b ORNs in the antennal lobes. a, c, and d) Confocal images of representative brains from a genetic screen to identify adhesion molecules involved in the glomerular organization of the Drosophila olfactory receptor neuron axon terminals. We crossed a second chromosome containing four different Drosophila olfactory receptor promoter-driven *GAL4s* (*Or47a-GAL4*, *Or47b-GAL4*, *Or23a-GAL4*, *Gr21a-GAL4*) together with a *UAS-Syt.GFP* reporter (*4xOr-GAL4 > Syt.GFP*) to the indicated *UAS-RNAi* lines or *attP40* background flies. The parental driver chromosome over the *CyO* balancer was used as a no-RNAi control. The invading Or47b ORN axons are denoted with white arrowheads. b) Summary of the phenotypical results from the genetic screen focusing on *beat/side* gene families. The Bloomington stock number and the transgenic docking site of each line are also listed. e and f) Schematic in (e) shows the genotype of animals used in (f), where each fly has one copy of the second chromosome carrying an *Or47b-GAL4* driver and a *UAS-Syt.GFP* reporter, and one copy of the indicated second chromosome, either a *CyO* balancer or *attP40* docking site derivatives. *attL* and *attR* sites are generated as a result of transgene integration into *attP40* docking site. Confocal images of representative brains are shown in (f). g) Confocal brain images of the indicated genotypes. (h and i) Schematic in (h) shows the genotype of animals used in (i), where each fly has one copy of the second chromosome *UAS-beat-Ia RNAi* transgene inserted into the *attP40* docking site, with one copy of *Or47b-GAL4 UAS-Syt.GFP*, either on the second or third chromosome. Confocal images of representative brains are shown in (i). 10–25 brains were examined in each genotype and the phenotypical penetrance is close to 100% in each *attP40*-derived group.

sequence was then amplified from the ligated genomic DNA by inverse PCR using forward and reverse primers targeting the 3′- or 5′-end sequences of the P-element (Fig. 3c). PCR reaction: 10 μl ligated DNA, 2 μl 5 μM forward and reverse primer mix, 10 μl 5X *myTaq* reaction buffer, 0.5 μl *Taq* DNA polymerase. Thermal cycling programme: 3 min initial denaturation at 95°C + 35 cycles (30 s denaturation at 95°C, 1 min annealing at 55°C, 2 min extension at 72°C) + 10 min final extension at 72°C. PCR products were then cleaned with Qiagen QIAquick PCR purification kit followed by commercial DNA sequencing service. Primers are listed in Table 1.

A genomic region on the second chromosome (starting from 2L: 2753160) within the first intron of *Bacc* gene was identified (Fig. 3, d and e) as the immediate sequence flanking the inserted P-element
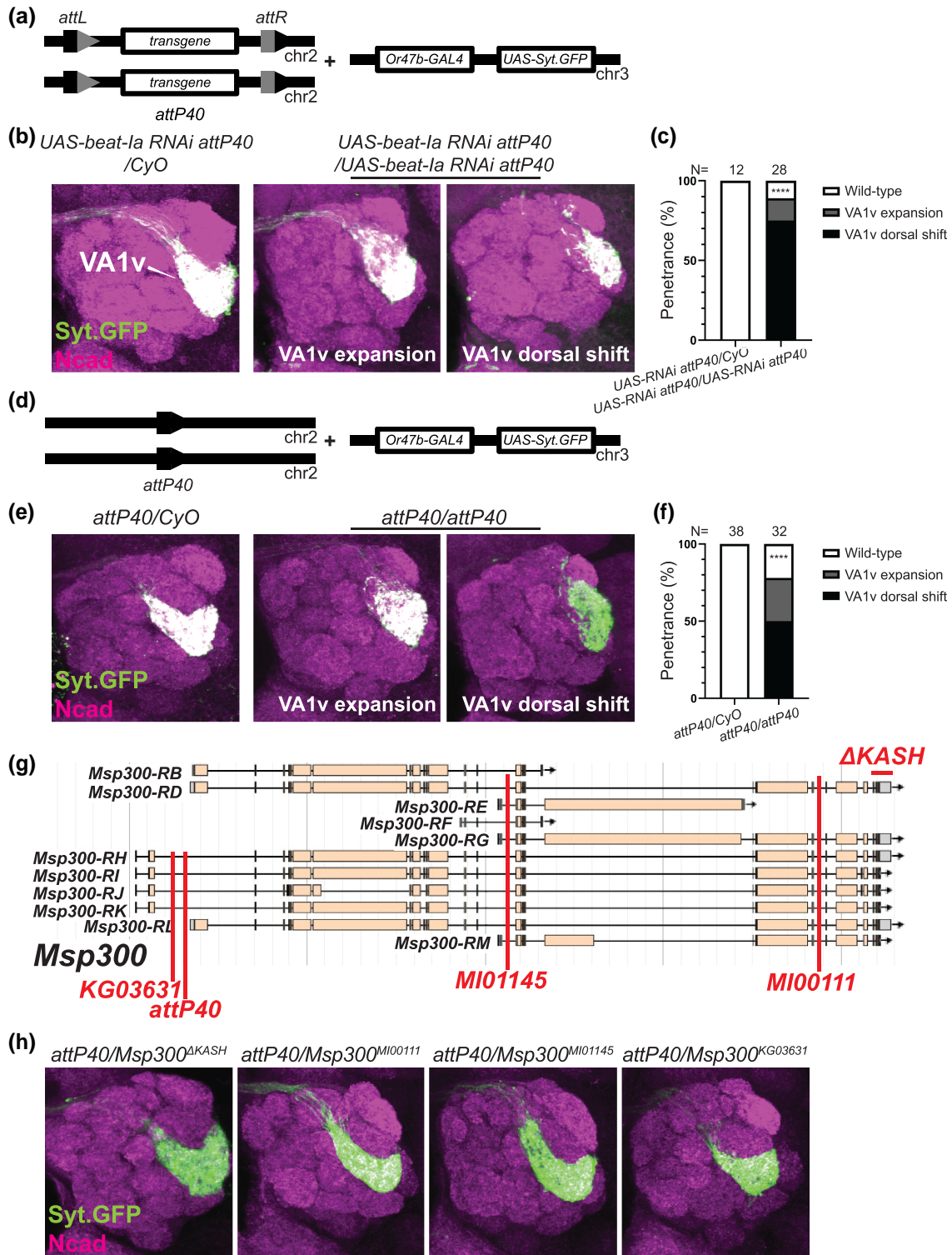
Fig. 2. Homozygous *attP40* chromosome affects glomerular organization of Or47b ORNs independent of the *Msp300* function. a–c) Schematic in (a) shows the genotype of animals used in (b), where each fly has one or two copies of the second chromosome *UAS-beat-Ia RNAi* transgene inserted at the *attP40* docking site, with the third chromosome *Or47b-GAL4 UAS-Syt.GFP* transgenes. Confocal images of representative brains are shown in (b). The percentage of the phenotypes is shown in (c). ****$P < 0.0001$ after Fisher's exact test. d–f) Schematic in (d) shows the genotype of animals used in (e), where each fly has one or two copies of the second chromosome empty *attP40* docking site, with the third chromosome *Or47b-GAL4 UAS-Syt.GFP* transgenes. Confocal images *of* representative brains are shown in (e). The percentage of the phenotypes is shown in (f). ****$P < 0.0001$ after Fisher's exact test. N in (c) and (f) denotes the antennal lobes examined. g) Schematic showing the *Msp300* genomic locus, the *attP40* docking site, three insertional *Msp300* mutations (*Msp300*^MI00111^, *Msp300*^MI01145^, *Msp300*^KG03631^), and one deletion allele (*Msp300*^ΔKASH^), each denoted with red lines. h) Confocal images of representative brains of the indicated transheterozygous animals, with the *attP40* docking site over the indicated *Msp300* alleles. N = 11, 8, 4, 12 brains in each genotype group, from left to right.
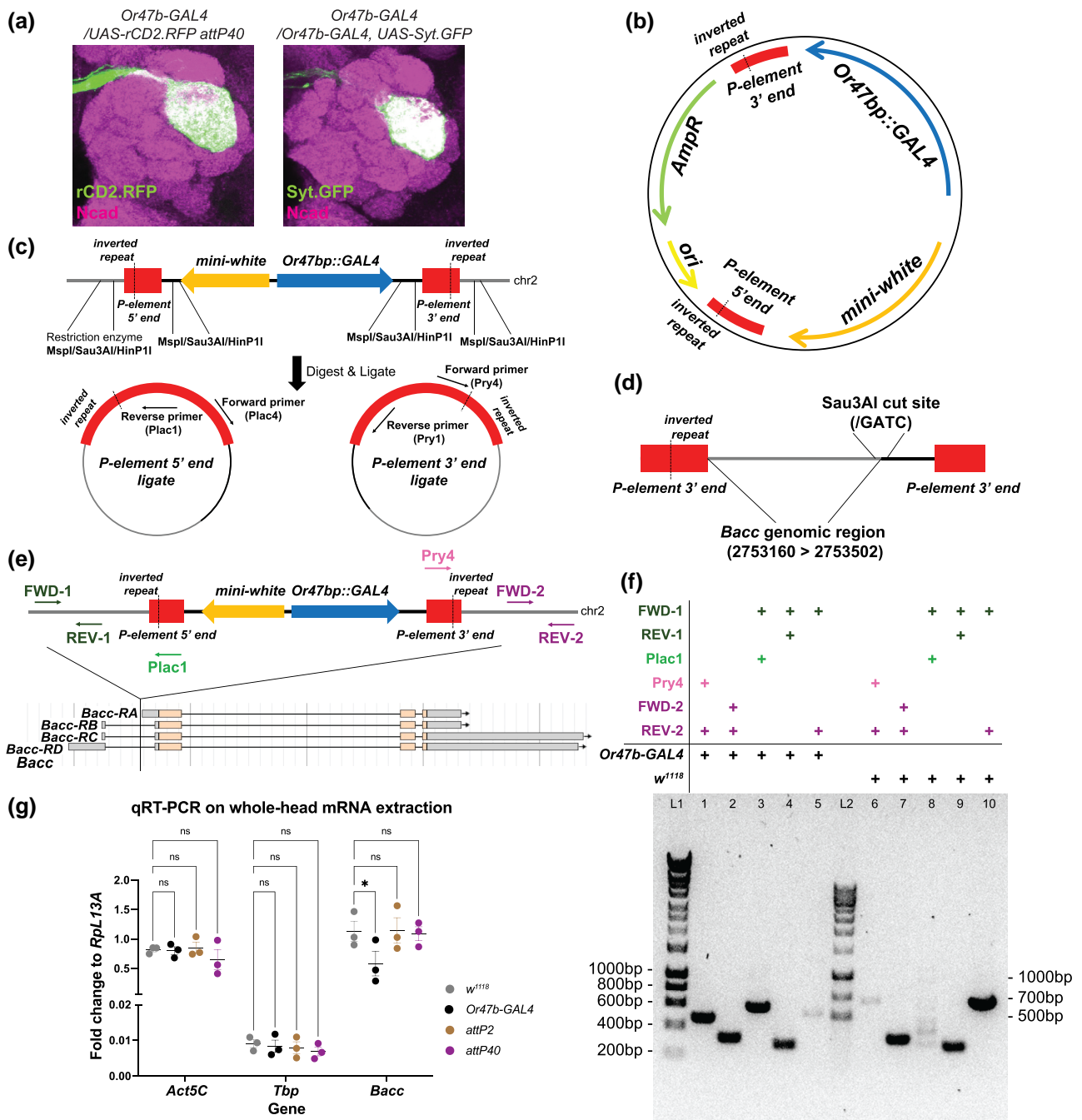
Fig. 3. Identification of the *Or47b-GAL4* transgene insertion site. a) Confocal images of the indicated genotypes suggesting the second chromosome *Or47b-GAL4* transgene is accounting for the glomerular expansion phenotype. N = 16 brains in each genotype and the phenotypical penetrance is 100%. b) The structure of the P-element vector containing *Or47b-GAL4* transgene (*Or47b* promoter fused with GAL4 coding sequence, denoted as *Or47bp::GAL4* in this and other panels of this figure) and a *mini-white* selectable marker. c) Schematic illustrating the recovery of genomic sequences flanking P-element insertion by inverse PCR. d) Schematic showing the sequencing results from one ligated genomic DNA template digested by Sau3AI restriction enzyme. A region within *Bacc* gene was recovered as the immediate sequencing flanking the 3′ end of the inserted P-element containing *Or47b-GAL4* transgene. e) Schematic showing the P-element insertion site within the first intron of *Bacc* gene. The arrows indicate the primers used in a PCR assay to validate this insertion. f) DNA gel showing the amplicons by each indicated primer pairs from *Or47b-GAL4* transgenic flies or w^{1118} control flies. Primer pairs FWD-1/ REV-1 and FWD-2/REV-2 can amplify the specific fragments from both *Or47b-GAL4* transgenic flies and w^{1118} control flies as expected because the corresponding sequences exist in both. Primer pairs FWD-1/Plac1 and Pry4/REV-2 only amplify specific products from *Or47b-GAL4* transgenic flies while fail to work from w^{1118} control flies as one primer in each pair targets the sequence of P-element which is not present in w^{1118} flies. Primer pair FWD-1/ REV-2 works in w^{1118} control flies but fails in *Or47b-GAL4* flies as the expected amplicon is too long to be amplified in transgenic animals because of the integration of large P-element sequence. g) qPCR results comparing the indicated gene expression levels normalized by *RpL13A* transcripts across different genotypes. ns, not significant. *P-value < 0.05 after two-way ANOVA followed by multiple comparison test. Error bars indicate mean ± SEM. N = 3 biological replicates per genotype. Each biological replicate contain 14~20 fly heads from equal number of males and females.

Table 1. Primers used in this study.

Experiment	Primer	Sequence (5′ to 3′)	Source
Inverse PCR	*For amplify P-element 3′-end flanking region*		(Huang *et al.* 2009)
	Pry1	CCTTAGCATGTCCGTGGGGTTTGAAT	
	Pry4	CAATCATATCGCTGTCTCACTCA	
	For amplify P-element 5′-end flanking region		
	Plac1	CACCCAAGGCTCTGCTCCCACAAT	
	Plac4	ACTGTGCGTTAGGTCCTGTTCATTGTT	
Sequencing	*For sequencing P-element 3′-end product*		(Huang *et al.* 2009)
	Spep1	GACACTCAGAATACTATTC	
	For sequencing P-element 5′-end product		
	Sp1	ACACAACCTTTCCTCTCAACAA	
PCR Validation assay	FWD-1	GAGCACATATCGGTGGTTAG	This study
	REV-1	GGCCCATACAATACACTCAA	
	FWD-2	CGAGAGGCAGTGCTTAAATA	
	REV-2	CTTGAGATCGTCCTTGACAG	
qPCR	Bacc-F	AGGCTCTGGAGGAAATCA	This study
	Bacc-R	CCGGAACCGTCATCATTATC	
	Act5C-F	GGCGCAGAGCAAGCGTGGTA	(Zhao *et al.* 2020)
	Act5C-R	GGGTGCCACACGCAGCTCAT	
	RpL13A-F	GCGAGGAGCTGAACCTCTC	
	RpL13A-R	GGAAGTGGAATGGACCACGG	
	Tbp-F	TAAGCCCCAACTTCTCGATTCC	
	Tbp-R	GCCAAAGAGACCTGATCCCC	

3′ end. To verify this identified genomic insertion site, a PCR assay was designed to amplify the genomic regions from *Or47b-GAL4* transgenic flies and w^{1118} control flies respectively with different primer pairs (Fig. 3, e and f). PCR mix recipe and thermal cycling programmes were the same as abovementioned. Amplicons were also purified and sequenced for validation.

Quantitative reverse transcription-PCR

To measure whether the insertion of *Or47b-GAL4* transgene into *Bacc* gene locus affects its expression, we used the quantitative reverse transcription-PCR (qRT-PCR) to extract and quantify the mRNA levels from whole heads of fruit flies. RNA extraction, cDNA preparation, and qPCR protocols were described previously (Zhao *et al.* 2020; Deanhardt *et al.* 2022).

Briefly, for each biological replicate, equal number of male and female heads (7 to 10, 5–7 days old post eclosion) were dissected in RNase-free environment with Trizol, followed by tissue homogenization, cell lysis, and filtration with Qiagen QIAshredder spin column. Three biological replicates were analyzed for each genotype. RNA was then extracted and purified by Qiagen RNeasy Kit per manufacturer's instructions and eluted in 60 μl RNase-free water. Genomic DNA was then removed using Invitrogen TURBO DNA-free Kit per manufacturer's instructions. RNA concentration was measured using NanoDrop after DNase treatment. Reverse transcription was performed by Invitrogen SuperScript IV First-Strand cDNA synthesis Reaction Kit per manufacturer's instructions. Notably, approximately equal amount of template RNA across different samples were added based on RNA concentration.

Lastly, qPCR reactions were run on Roche LightCycler 96 Instrument with FastStart Essential DNA Green Master (2X) in 20 μl volume with technical triplicates per manufacturer's instructions. Thermal cycling programme: 600 s pre-incubation at 95°C + 40 three-step amplification cycles (10 s denaturation at 95°C, 10 s annealing at 55°C, 15 s extension at 72°C with Single acquisition) + Melting Curve (10 s 95°C, 60 s 65°C, 1 s 97°C with 5 Readings/°C). qPCR primers were designed to span two adjacent exons when possible, with target amplicon length of 120 bp. Primer pairs were tested to generate standard curves to evaluate amplification efficiency before being used for expression comparison experiments. Expression levels of the gene of interest were normalized to the house keeping gene *RpL*13A in each sample by $2^{-\Delta Ct}$ method. Two-way ANOVA followed by multiple comparison test was performed in Prism 9 software to determine statistical significance. Primers are listed in Table 1.

Results

We used the *Drosophila* olfactory receptor neurons (ORNs) as a model to understand the molecular mechanisms underlying neuronal circuit assembly. In *Drosophila*, each class of ORNs expresses a unique olfactory receptor (*Or*) gene, and ORN axons target to the brain antennal lobe within class-specific and uniquely positioned synaptic units called glomeruli (Hong and Luo 2014; Barish and Volkan 2015). To identify the molecular players contributing to the glomerular organization of the ORNs, we genetically screened genes encoding cell adhesion molecules whose expression levels increase over pupal development in the antennae (Barish *et al.* 2018). Among these, *beat* and *side* gene families drew our attention because they encode the Ig superfamily proteins, form a heterophilic interacting protein network, and have been previously revealed to be involved in neuronal adhesion (Fambrough and Goodman 1996; Pipes *et al.* 2001; Sink *et al.* 2001; de Jong *et al.* 2005; Siebert *et al.* 2009; Özkan *et al.* 2013; Li *et al.* 2017; Kinold *et al.* 2021). We obtained a collection of transgenic *UAS-RNAi* lines from TriP library deposited at the Bloomington Drosophila Stock Center (BDSC) and crossed these lines with an established recombinant chromosome containing four different *Or* promoter-driven *GAL4* transgenes (*Or47a-GAL4*, *Or47b-GAL4*, *Or23a-GAL4*, *Gr21a-GAL4*, *4xOr-GAL4* for short, Fig. 1 a–d) together with a *UAS-Syt.GFP* reporter. We examined the knockdown effect of candidate genes on axonal targeting of these four ORN classes. The parent flies with a single copy of the *GAL4* drivers showed wild type glomerular organization (Fig. 1a). As an additional control, we also crossed *GAL4* driver lines to flies expressing the RNAi against a red fluorescent protein (RFP) mCherry, which also exhibited no apparent defect in glomerular organization (Fig. 1a).

From the screen, we found a strikingly recurrent phenotype, where the axon terminals of Or47b ORNs invade the neighbouring

region, leading to an expanded round VA1v glomerulus in contrast to the crescent shape in control brains (Fig. 1a). This phenotype was observed in two independent RNAi lines targeting the same gene, for example, *beat-Ia* (Fig. 1a). However, screening a list of *beat* and *side* family members revealed a pattern for the phenotype, which only correlated with the second chromosome *UAS-RNAi* transgenes, independent of the gene identity. Figure 1b summarizes the screening results from *beat/side* gene families. All the RNAi lines inserted at the second chromosome *attP40* site yielded the expanded VA1v glomerulus phenotype, whereas none of the RNAi lines inserted at the third chromosome *attP2* site showed this defect. Notably, there is one gene, *beat-IIIc*, with one *attP40*-derived RNAi line and one *attP2*-derived RNAi line. Only the *attP40 UAS-RNAi* insertion gave rise to the phenotype (Fig. 1b). The same phenotype was also observed with randomly selected TRiP *UAS-RNAi* lines inserted at the *attP40* site targeting genes without known roles in ORN development (Supplementary Figure 1, a and b). To test whether this phenotype is caused by specific effects of RNAi-mediated gene knockdown or simply by the presence of *attP40*-derived insertions, we first crossed the same *Or47b-GAL4* driver line to a third *UAS-RNAi* line from Vienna Drosophila Resource Center (VDRC) targeting *beat-Ia*, which was generated by random P-element-mediated insertions (Dietzl *et al.* 2007). This non-*attP40 UAS-RNAi* line could not reproduce the phenotype obtained by the *attP40*-derived *UAS-RNAi* from the TRiP collection (Fig. 1c). In addition, crossing the driver line to an empty *attP40* site without any transgenes led to the same glomerular expansion phenotype (Fig. 1d). These results suggest that the Or47b ORN-specific VA1v glomerular defect is independent of the RNAi-based knockdown of the genes examined but caused by an effect from the *attP40*-derived chromosome.

Since we repeatedly obtained the VA1v glomerular phenotype with the second chromosome *Or47b-GAL4*-driven *UAS-RNAi*, we also tested if crossing flies carrying the same *Or47b-GAL4* transgene to various *attP40* derivatives could result in the same phenotype (Fig. 1e). Compared with the no *attP40* control (over a *CyO* balancer chromosome), the *attP40* landing site with and without *UAS-RNAi* insertion, or a ubiquitous promoter-driven gRNA targeting the *QUAS* sequence (control gRNA) all produced the same VA1v glomerular defect when crossed to the second chromosome *Or47b-GAL4*-driven *UAS-Syt.GFP* (Fig. 1f). We also crossed *Or47b-GAL4 UAS-Syt.GFP* chromosome to three lines carrying *UAS-rCD2.RFP* transgenic insertion at three different chromosomal locations, *attP2* (on chr3), *attP5* (on chr2R), and *attP40* (on chr2L). Only *Or47b-GAL4* over *UAS-rCD2.RFP* insertion at *attP40* resulted in glomerular expansion phenotype while the insertions at *attP2* and *attP5* appeared wild type. These results again suggest that the VA1v glomerular defect is uniquely linked to the *attP40*-associated insertions and is independent of the transgene or other attP landing sites.

The glomerular organization defect could be caused by simply the presence of *attP40* insertion or the genetic interaction between the *attP40* background and the chromosome carrying the reporter transgene. To distinguish between these possibilities, we examined the animals carrying a single copy of *attP40* insertion and a different *Or47b-GAL4 UAS-Syt.GFP* reporters on the third chromosome. In these animals, VA1v glomerulus appeared normal (Fig. 1, h and i). The observation that a single copy of *attP40* is not sufficient to produce a glomerular phenotype indicates that the *attP40* effects on VA1v glomerulus are not dominant. Rather, they point to a combinatorial effect of the second chromosome with *Or47b-GAL4 UAS-Syt.GFP* over the chromosome with the empty or transgene-carrying *attP40* docking site on the glomerular

phenotype (Fig. 1, h and i). Thus, we conclude that the *attP40* chromosome genetically interacts with the second chromosome reporters to disrupt VA1v glomerular organization.

As the *attP40* effect appears to be recessive, we next examined if animals homozygous for the *attP40* sites display any VA1v glomerular defects. To bypass the glomerular defects arising from the genetic interactions between *attP40* and the second chromosome reporters, we used the third chromosome *Or47b-GAL4 UAS-Syt.GFP* reporter to visualize VA1v glomerulus. Surprisingly, homozygous *attP40* derivatives or *attP40* empty docking site alone produced strong axon terminal defects (Fig. 2 a–f). In contrast, flies heterozygous for the *attP40* site with or without transgenes inserted appeared wild type (Fig. 2 a–f). Most of the brains homozygous for the *attP40* site with or without insertions displayed a dorsally positioned VA1v glomerulus (Fig. 2, b and e, middle panels; Fig. 2, c and f), whereas a small proportion also exhibited an expanded glomerulus (Fig. 2, b and e, right panels; Fig. 2, c and f). Given that the *attP40* site is located within an intron of *Msp300* gene, we posited that it likely disrupts *Msp300* function. *Msp300* encodes a Nesprin-like protein, which is required for proper positioning of muscle nuclei and neuromuscular junction formation (Elhanany-Tamir *et al.* 2012; Morel *et al.* 2014). Single-cell RNA-seq datasets from ORNs also show broad expression of *Msp300* across ORN classes (Li *et al.* 2022). We thus tested if the VA1v glomerular defect is caused by the loss of *Msp300* function. We analyzed transheterozygotes of empty *attP40* docking site over other mutant alleles of *Msp300*, such as *Msp300^{AKASH}* (which lacks the KASH domain [Xie and Fischer 2008; Elhanany-Tamir *et al.* 2012]), *Msp300^{MI00111}*, *Msp300^{MI01145}* [two MIMIC-based alleles predicted to disrupt most splice isoforms of *Msp300* transcripts (Venken *et al.* 2011)], and *Msp300^{KG03631}* [a P-element-based insertion which is close to *attP40* landing site (Bellen *et al.* 2004)] (Fig. 2g). However, none of these genetic combinations recapitulated VA1v glomerular phenotype (Fig. 2h). This indicates that the VA1v glomerular defect is independent of the *Msp300* function and is likely caused by other genes nearby affected by the *attP40* insertion or a second recessive mutation linked to the *attP40* docking site.

We next sought to figure out the molecular basis of the genetic interaction between that specific *Or47b-GAL4*-bearing chromosome and *attP40* chromosome. Flies transheterozygous for *attP40* (empty or with insertions) over *4xOr-GAL4 UAS-Syt.GFP* or *Or47b-GAL4 UAS-Syt.GFP* robustly exhibit VA1v glomerular phenotype. We infer that the putative genetic lesion is directly caused by or genetically linked to the *Or47b-GAL4* transgene for three reasons: (1) a farther second site mutation would likely be lost during meiotic recombination events to generate these stocks; (2) this *Or47b-GAL4* recombined with other *UAS-reporters*, *UAS-mCD8.GFP* or *UAS-RFP*, over the *attP40* derivatives exhibited the same phenotype (Supplementary Figure 2); and (3) crossing the second chromosome *Or47b-GAL4* transgene alone to the *UAS-rCD2.RFP* reporter inserted at *attP40* also reproduced the expanding glomerulus (Fig. 3a), which rules out the confounding effect from *UAS-Syt.GFP* transgene. Indeed, two copies of this *Or47b-GAL4* chromosome also results in similar glomerular phenotypes (Fig. 3a). *Or47b-GAL4* transgene was generated by P-element-mediated genomic integration (Fig. 3b) and the exact site of the insertion was not mapped (Vosshall *et al.* 2000). We used inverse PCR (Huang *et al.* 2009) to identify the insertion site and determine the gene whose function is potentially disrupted (Fig. 3c). We successfully recovered a piece of genomic sequence immediately flanking the 3′ end of the inserted P-element, which is within the first intron of *Bacc* gene (chr2L:2753160, Fig. 3, d and e) and also a P-element insertion-enriched region. We performed

genomic PCR to further validate the *Bacc* intronic insertion from both 3′ and 5′ ends of the P-element using different primer pairs targeting the P-element ends and flanking *Bacc* sequences (Fig. 3e). We amplified the desired DNA fragments from *Or47b-GAL4*-bearing flies but not from w^{1118} flies (Fig. 3, e and f). In addition, primer pairs targeting only *Bacc* sequences flanking the insertion amplified the expected fragment only from w^{1118} files but not from *Or47b-GAL4* flies (Fig. 3, e and f). We next tested if this intronic insertion affects *Bacc* transcriptional levels using Quantitative Reverse Transcription-PCR (qRT-PCR). We extracted mRNA from whole heads of the adult *Or47b-GAL4* homozygotes, as well as homozygous *attP2*, *attP40*, and w^{1118} adults. qRT-PCR results showed that *Bacc* transcripts normalized to the housekeeping gene *RpL13A* decrease by ∼two fold in flies homozygous for *Or47b-GAL4* but are not significantly altered in *attP2* or *attP40* animals compared to w^{1118} controls (Fig. 3g). In contrast, other housekeeping genes *Act5C* and *Tbp* remain unchanged across these genotypes (Fig. 3g). These results indicate that: (1) second chromosome *Or47b-GAL4* transgene insertion disrupts *Bacc* gene function and (2) homozygous and transheterozygous combinations of *Or47b-GAL4* and *attP40* backgrounds likely utilize distinct mechanisms to disrupt VA1v glomerular organization.

Discussion

Here, we found that homozygous *attP40* chromosome leads to defective glomerular organization of ORNs. This defect is likely not caused by the loss of *Msp300* function, where the *attP40* site is inserted. Moreover, the *attP40* chromosome genetically interacts with a second chromosome carrying the *Or47b-GAL4* transgene, resulting in a similar ORN axon terminal defect. Though the exact genetic reasons and molecular mechanisms are unknown, our finding raises the critical issue with using this popular transgene landing site. Rigorous controls are needed to rule out the *attP40*-associated background effects, as discussed below.

The genetics underlying the Or47b ORN phenotypes

A recent study reported that flies homozygous for the *attP40*-derived insertions had 50% reduction in *Msp300* transcript levels and phenocopied the defects in larval muscle nuclei clustering in *Msp300* mutants (van der Graaf *et al.* 2022). As homozygotes of the *attP40* chromosome are defective in Or47b ORN axon terminal organization, we hypothesized that the *attP40*-affected *Msp300* gene is responsible for the defect. However, this is not the case as *attP40* over various *Msp300* mutations appeared phenotypically wild type, suggesting the *attP40* chromosome may carry an unannotated mutation responsible for *Msp300*-independent ORN glomerular disorganization.

The *attP40* docking site with or without transgene insertions may also disrupt other genes in the vicinity of *Msp300*. For example, in addition to *Msp300, attP40* docking site is flanked on the opposing side by *ND-13A,* which encodes a component of the mitochondria electron transport chain complex I. Thus, the *attP40* docking site alone or with transgene insertions may lead to a variety of phenotypes as a result of disrupted *ND-13A*. Indeed, Groen *et al.* reported that *attP40* flies exhibit resistance to cisplatin-induced neuronal damage mediated by the reduced expression of *ND-13A* (Groen *et al.* 2022). Whether the glomerular defect is dependent on the *ND-13A* function is beyond the scope of this paper but needs to be tested in the future studies.

Surprisingly, we found transheterozygous animals with an *attP40* chromosome over the second chromosome *Or47b-GAL4* transgene produced similar but not identical glomerular abnormalities to *attP40* homozygotes. Additionally, *Or47b-GAL4* homozygotes exhibit comparable phenotypes with *Or47b-GAL4/attP40* transheterozygotes. These suggest several possible underlying genetic mechanisms: (1) *Or47b-GAL4* and *attP40* backgrounds harbour common mutations; (2) *Or47b-GAL4* and *attP40* backgrounds possess completely separate genetic lesions that genetically interact. The genetic interaction model is favoured due to qualitatively distinguishable phenotypes between *Or47b-GAL4/attP40* animals and *attP40/attP40* ones. Furthermore, *Or47b-GAL4* transgene is inserted into an intron of *Bacc* gene, which encodes a tyramine-dependent nuclear regulator (Chen *et al.* 2013), reducing its expression levels by about 50% in homozygotes. No change in transcript levels were observed in *attP40* homozygotes. *Bacc* mRNAs are abundant in brain tissues, comparable to housekeeping genes *Act5C* and *RpL13A* (Fig. 3g). Our results imply its potential novel role in ORN axon pathfinding or glomerular patterning. Future functional studies will determine whether the disruption of *Bacc* expression is causative to the VA1v glomerular phenotype and the mechanisms by which *Bacc* mutations and their genetic interactors in the *attP40* background result in glomerular defects.

Unique genetic sensitivity of VA1v glomerulus architecture

One of the most peculiar observations from our study is that Or47b ORNs seem to be particularly sensitive to changes in genetic background. In fact, VA1v glomerular disruptions are not only restricted to the *attP40* background, but can be seen in many other mutants with effects on ORN axon and synapse organization in the antennal lobes (Ang *et al.* 2003; Yao *et al.* 2007; Hong *et al.* 2012; Li *et al.* 2013; Hueston *et al.* 2016; Wu *et al.* 2017; Xie *et al.* 2019; Hing *et al.* 2020). In addition to the variability of VA1v glomerular architecture to genetic background effects, pheromone sensing Or47b ORNs and the trichoid at4 sensillum that houses Or47b, Or88a, and Or65a/b/c ORNs are developmentally special. At4 sensillum appears to be a developmentally default state for all trichoid sensilla. For example, loss of transcription factor Rn function, normally expressed in at1 and at3 ORNs, leads to a loss of at1 and at3 sensilla identity, and their conversion to at4 sensillum identity (Li *et al.* 2013, 2015, 2016). Similarly, Or47b ORNs in at4 sensillum appear to have a default identity, as mutants in *Alh,* a chromatin factor, result in the conversion of Or88a and Or65a ORNs to Or47b ORN fate (Hueston *et al.* 2016). In addition to these findings that point to a developmentally special state for pheromone sensing Or47b ORNs or "at" sensilla, the glomeruli targeted by the trichoid ORNs are morphologically plastic. In Drosophila, they are sexually dimorphic, appearing larger in males (Stockinger *et al.* 2005). In insects such as moths trichoid glomeruli can form separate macro-glomerular complex outside the antennal lobe of male brains (Berg *et al.* 1998). Given the developmental plasticity of trichoid pheromone sensing ORNs and the developmental ground state of at4 sensilla, Or47b developmental trajectory might be particularly sensitive to genetic background effects to accommodate adaptive developmental, behavioural and evolutionary processes. On the other hand, we only examined Or47b VA1v glomerulus in the *attP40* background, and *attP40* homozygotes possibly display structural defects in other ORN classes and their glomeruli. Future studies will help identify these phenotypes and the genetic lesions leading to *attP40*-associated phenotypes.

Addressing genetic background issues when using genetic reagents

To summarize, we found unexpected background effects of the *Drosophila attP40* landing site on the ORN glomerular organization. In parallel with other recent studies reporting other phenotypes arising from the *attP40* background, ranging from muscle development to neuronal stress responses, such background effects should be seriously considered in using *attP40*-derived flies. It is recommended to avoid using homozygotes/double-copies of the *attP40*-based insertions. Researchers should also be aware of the potential genetic interactions between the *attP40*-bearing chromosome and the other homologous second chromosomes even if it does not contain any *attP40* derivatives. Appropriate controls should be applied to override these caveats. For example, when working with *GAL4/UAS-effector* binary system, it is better to use a *GAL4*-driven *UAS-neutral effector* (such as *UAS-RNAi* against neutral or non-fly genes inserted at the same docking site) as a negative control, rather than the widespread use of *GAL4* alone or *UAS-effector* alone controls. Transgenic rescue of RNAi-based gene knockdowns is not feasible due to targeting of rescue transgenes by the RNAi. Thus, use of full animal mutants or MARCM based clonal mutant analysis should be coupled with RNAi-based phenotypic analyses. Though the underlying genetic reasons remain elusive, studies demonstrated that the *attP40* landing site on the second chromosome affects the expression of multiple genes (Groen *et al.* 2022; van der Graaf *et al.* 2022). Additional omics-based experiments in the future will be needed to determine all the genetic lesions in *attP40* strains that underly many phenotypic defects observed in this background. These studies will also reveal potential genetic alterations associated with glomerular defects, providing new insights into ORN axon pathfinding and glomerular organization.

Data availability

The authors affirm that all the data necessary for drawing the conclusions are present in the text, figures, and figure legends. Most of the *Drosophila* stocks are obtained from Bloomington or Vienna Stock center, with identifiers listed in the Materials and methods section. All the other lines are available upon request.

Supplemental material available at G3 online.

Conflicts of interest

The authors declare no conflict of interest.

Author contributions

Q.D. and P.C.V. conceived the study and designed the experiments; Q.D. did most of the experiments with help from R.E., A.C., and Y.C.; Q.D. analyzed the data and prepared the figures; Q.D. and P.C.V. wrote and edited the manuscript.

Literature cited

Ang LH, Kim J, Stepensky V, Hing H. Dock and Pak regulate olfactory axon pathfinding in Drosophila. Development. 2003;130(7): 1307–1316. doi:10.1242/dev.00356.

Barish S, Nuss S, Strunilin I, Bao S, Mukherjee S, *et al.* Combinations of DIPs and Dprs control organization of olfactory receptor neuron terminals in Drosophila. PLoS Genet. 2018;14(8):e1007560. doi:10.1371/journal.pgen.1007560.

Barish S, Volkan PC. Mechanisms of olfactory receptor neuron specification in Drosophila. Wiley Interdiscip Rev Dev Biol. 2015;4(6): 609–621. doi:10.1002/wdev.197.

Bellen HJ, Levis RW, Liao G, He Y, Carlson JW, *et al.* The BDGP gene disruption project: single transposon insertions associated with 40% of Drosophila genes. Genetics. 2004;167(2):761–781. doi:10. 1534/genetics.104.026427.

Berg B, Almaas T, Bjaalie J, Mustaparta H. The macroglomerular complex of the antennal lobe in the tobacco budworm moth *Heliothis virescens*: specified subdivision in four compartments according to information about biologically significant compounds. J Comp Physiol A. 1998;183(6):669–682. doi:10.1007/ s003590050290.

Brand AH, Perrimon N. Targeted gene expression as a means of altering cell fates and generating dominant phenotypes. Development. 1993;118(2):401–415. doi:10.1242/dev.118.2.401.

Chen J, Wang Y, Zhang Y, Shen P. Mutations in bacchus reveal a tyramine-dependent nuclear regulator for acute ethanol sensitivity in Drosophila. Neuropharmacology. 2013;67:25–31. doi:10. 1016/j.neuropharm.2012.10.013.

Deanhardt B, Duan Q, Du C, Soeder C, Morlote A, *et al.* Social experience and pheromone receptor activity reprogram behavioral switch and neuromodulatory gene expression in sensory neurons. bioRxiv 449021. doi:10.1101/2021.06.18.449021, 16 August 2022, preprint: not peer reviewed.

de Jong S, Cavallo JA, Rios CD, Dworak HA, Sink H. Target recognition and synaptogenesis by motor axons: responses to the sidestep protein. Int J Dev Neurosci. 2005;23(4):397–410. doi:10.1016/j. ijdevneu.2004.10.002.

Dietzl G, Chen D, Schnorrer F, Su K-C, Barinova Y, *et al.* A genome-wide transgenic RNAi library for conditional gene inactivation in Drosophila. Nature. 2007;448(7150):151–156. doi:10.1038/ nature05954.

Elhanany-Tamir H, Yu YXV, Shnayder M, Jain A, Welte M, *et al.* Organelle positioning in muscles requires cooperation between two KASH proteins and microtubules. J Cell Biol. 2012;198(5): 833–846. doi:10.1083/jcb.201204102.

Fambrough D, Goodman CS. The Drosophila beaten path gene encodes a novel secreted protein that regulates defasciculation at motor axon choice points. Cell. 1996;87(6):1049–1058. doi:10. 1016/S0092-8674(00)81799-7.

Fishilevich E, Vosshall LB. Genetic and functional subdivision of the Drosophila antennal lobe. Curr Biol. 2005;15(17):1548–1553. doi: 10.1016/j.cub.2005.07.066.

Gaudet P, Livstone MS, Lewis SE, Thomas PD. Phylogenetic-based propagation of functional annotations within the gene ontology consortium. Brief Bioinform. 2011;12(5):449–462. doi:10.1093/ bib/bbr042.

Green EW, Fedele G, Giorgini F, Kyriacou CP. A Drosophila RNAi collection is subject to dominant phenotypic effects. Nat Methods. 2014;11(3):222–223. doi:10.1038/nmeth.2856.

Groen CM, Podratz JL, Pathoulas J, Staff N, Windebank AJ. Genetic reduction of mitochondria complex I subunits is protective against cisplatin-induced neurotoxicity in *Drosophila*. J Neurosci. 2022; 42(5):922–937. doi:10.1523/JNEUROSCI.1479-20.2021.

Groth AC, Fish M, Nusse R, Calos MP. Construction of transgenic Drosophila by using the site-specific integrase from phage φC31. Genetics. 2004;166(4):1775–1782. doi:10.1534/genetics.166.4. 1775.

Hing H, Reger N, Snyder J, Fradkin LG. Interplay between axonal Wnt5-Vang and dendritic Wnt5-Drl/Ryk signaling controls glomerular patterning in the Drosophila antennal lobe. PLoS Genet. 2020;16(5):e1008767. doi:10.1371/journal.pgen.1008767.

Hong W, Luo L. Genetic control of wiring specificity in the fly olfactory system. Genetics. 2014;196(1):17–29. doi:10.1534/genetics. 113.154336.

Hong W, Mosca TJ, Luo L. Teneurins instruct synaptic partner matching in an olfactory map. Nature. 2012;484(7393):201–207. doi:10.1038/nature10926.

Housden BE, Muhar M, Gemberling M, Gersbach CA, Stainier DY, *et al.* Loss-of-function genetic tools for animal models: cross-species and cross-platform differences. Nat Rev Genet. 2017;18(1): 24–40. doi:10.1038/nrg.2016.118.

Huang AM, Rehm EJ, Rubin GM. Recovery of DNA sequences flanking P-element insertions in Drosophila: inverse PCR and plasmid rescue. Cold Spring Harb Protoc. 2009;2009(4):pdb.prot5199. doi:10. 1101/pdb.prot5199.

Hueston CE, Olsen D, Li Q, Okuwa S, Peng B, *et al.* Chromatin modulatory proteins and olfactory receptor signaling in the refinement and maintenance of fruitless expression in olfactory receptor neurons. PLoS Biol. 2016;14(4):e1002443. doi:10.1371/journal. pbio.1002443.

Kinold JC, Brenner M, Aberle H. Misregulation of Drosophila sidestep leads to uncontrolled wiring of the adult neuromuscular system and severe locomotion defects. Front Neural Circuits. 2021;15: 658791. doi:10.3389/fncir.2021.658791.

Larkin A, Marygold SJ, Antonazzo G, Attrill H, dos Santos G, *et al.* Flybase: updates to the Drosophila melanogaster knowledge base. Nucleic Acids Res. 2020;49(D1):D899–D907. doi:10.1093/ nar/gkaa1026.

Li Q, Barish S, Okuwa S, Maciejewski A, Brandt AT, *et al.* A functionally conserved gene regulatory network module governing olfactory neuron diversity. PLoS Genet. 2016;12(1):e1005780. doi:10. 1371/journal.pgen.1005780.

Li Q, Barish S, Okuwa S, Volkan PC. Examination of endogenous rotund expression and function in developing Drosophila olfactory system using CRISPR-Cas9-mediated protein tagging. G3 (Bethesda). 2015;5(12):2809–2816. doi:10.1534/g3.115.021857.

Li Q, Ha TS, Okuwa S, Wang Y, Wang Q, *et al.* Combinatorial rules of precursor specification underlying olfactory neuron diversity. Curr Biol. 2013;23(24):2481–2490. doi:10.1016/j.cub.2013.10.053.

Li H, Janssens J, De Waegeneer M, Kolluru SS, Davie K, *et al.* Fly cell atlas: a single-nucleus transcriptomic atlas of the adult fruit fly. Science. 2022;375(6584):eabk2432. doi:10.1126/science.abk2432.

Li H, Watson A, Olechwier A, Anaya M, Sorooshyari SK, *et al.* Deconstruction of the beaten path-sidestep interaction network provides insights into neuromuscular system development. Elife. 2017;6:e28111. doi:10.7554/eLife.28111.

Markstein M, Pitsouli C, Villalta C, Celniker SE, Perrimon N. Exploiting position effects and the gypsy retrovirus insulator to engineer precisely expressed transgenes. Nat Genet. 2008;40(4): 476–483. doi:10.1038/ng.101.

Morel V, Lepicard S, Rey AN, Parmentier M-L, Schaeffer L. Drosophila nesprin-1 controls glutamate receptor density at neuromuscular junctions. Cell Mol Life Sci. 2014;71(17):3363–3379. doi:10.1007/ s00018-014-1566-7.

Ni J-Q, Liu L-P, Binari R, Hardy R, Shim H-S, *et al.* A Drosophila resource of transgenic RNAi lines for neurogenetics. Genetics. 2009;182(4):1089–1100. doi:10.1534/genetics.109.103630.

Ni J-Q, Markstein M, Binari R, Pfeiffer B, Liu L-P, *et al.* Vector and parameters for targeted transgenic RNA interference in *Drosophila melanogaster*. Nat Methods. 2008;5(1):49–51. doi:10. 1038/nmeth1146.

Ni J-Q, Zhou R, Czech B, Liu L-P, Holderbaum L, *et al.* A genome-scale shRNA resource for transgenic RNAi in Drosophila. Nat Methods. 2011;8(5):405–407. doi:10.1038/nmeth.1592.

Özkan E, Carrillo RA, Eastman CL, Weiszmann R, Waghray D, *et al.* An extracellular interactome of immunoglobulin and LRR proteins reveals receptor-ligand networks. Cell. 2013;154(1):228–239. doi: 10.1016/j.cell.2013.06.006.

Perkins LA, Holderbaum L, Tao R, Hu Y, Sopko R, *et al.* The transgenic RNAi project at harvard medical school: resources and validation. Genetics. 2015;201(3):843–852. doi:10.1534/genetics.115. 180208.

Pipes GC, Lin Q, Riley SE, Goodman CS. The beat generation: a multigene family encoding IgSF proteins related to the beat axon guidance molecule in Drosophila. Development. 2001;128(22): 4545–4552. doi:10.1242/dev.128.22.4545.

Ramin M, Li Y, Chang WT, Shaw H, Rao Y. The peacefulness gene promotes aggression in Drosophila. Mol Brain. 2019;12(1):1. doi:10. 1186/s13041-018-0417-0.

Scott K, Brady R Jr, Cravchik A, Morozov P, Rzhetsky A, *et al.* A chemosensory gene family encoding candidate gustatory and olfactory receptors in Drosophila. Cell. 2001;104(5):661–673. doi:10.1016/ S0092-8674(01)00263-X.

Siebert M, Banovic D, Goellner B, Aberle H. Drosophila motor axons recognize and follow a sidestep-labeled substrate pathway to reach their target fields. Genes Dev. 2009;23(9):1052–1062. doi: 10.1101/gad.520509.

Sink H, Rehm EJ, Richstone L, Bulls YM, Goodman CS. Sidestep encodes a target-derived attractant essential for motor axon guidance in Drosophila. Cell. 2001;105(1):57–67. doi:10.1016/S0092-8674(01)00296-3.

Stockinger P, Kvitsiani D, Rotkopf S, Tirian L, Dickson BJ. Neural circuitry that governs Drosophila male courtship behavior. Cell. 2005;121(5):795–807. doi:10.1016/j.cell.2005.04.026.

Titlow J, Robertson F, Järvelin A, Ish-Horowicz D, Smith C, *et al.* Syncrip/hnRNP Q is required for activity-induced Msp300/ nesprin-1 expression and new synapse formation. J Cell Biol. 2020;219(3):e201903135. doi:10.1083/jcb.201903135.

van der Graaf K, Srivastav S, Singh P, McNew JA, Stern M. The Drosophila melanogaster attP40 docking site and derivatives are insertion mutations of msp-300. PLoS One. 2022;17(12): e0278598. doi:10.1371/journal.pone.0278598.

Venken KJ, Schulze KL, Haelterman NA, Pan H, He Y, *et al.* MiMIC: a highly versatile transposon insertion resource for engineering *Drosophila melanogaster* genes. Nat Methods. 2011;8(9):737–743. doi:10.1038/nmeth.1662.

Vissers JH, Manning SA, Kulkarni A, Harvey KF. A Drosophila RNAi library modulates hippo pathway-dependent tissue growth. Nat Commun. 2016;7(1):10368. doi:10.1038/ncomms10368.

Vosshall LB, Wong AM, Axel R. An olfactory sensory map in the fly brain. Cell. 2000;102(2):147–159. doi:10.1016/S0092-8674(00)00021-0.

Wu B, Li J, Chou YH, Luginbuhl D, Luo L. Fibroblast growth factor signaling instructs ensheathing glia wrapping of *Drosophila* olfactory glomeruli. Proc Natl Acad Sci U S A. 2017;114(29):7505–7512. doi: 10.1073/pnas.1706533114.

Xie X, Fischer JA. On the roles of the Drosophila KASH domain proteins Msp-300 and klarsicht. Fly (Austin). 2008;2(2):74–81. doi:10.4161/fly.6108.

Xie Q, Wu B, Li J, Xu C, Li H, *et al.* Transsynaptic fish-lips signaling prevents misconnections between nonsynaptic partner olfactory neurons. Proc Natl Acad Sci U S A. 2019;116(32):16068–16073. doi:10.1073/pnas.1905832116.

Yao Y, Wu Y, Yin C, Ozawa R, Aigaki T, *et al.* Antagonistic roles of Wnt5 and the Drl receptor in patterning the Drosophila antennal lobe. Nat Neurosci. 2007;10(11):1423–1432. doi:10.1038/nn1993.

Zhao S, Deanhardt B, Barlow GT, Schleske PG, Rossi AM, *et al.* Chromatin-based reprogramming of a courtship regulator by concurrent pheromone perception and hormone signaling. Sci Adv. 2020;6(21):eaba6913. doi:10.1126/sciadv.aba6913.

Zheng Y, Buchwalter RA, Zheng C, Wight EM, Chen JV, *et al.* A perinuclear microtubule-organizing centre controls nuclear positioning and basement membrane secretion. Nat Cell Biol. 2020;22(3):297–309. doi:10.1038/s41556-020-0470-7.

Zirin J, Hu Y, Liu L, Yang-Zhou D, Colbeth R, *et al.* Large-Scale transgenic *Drosophila* resource collections for loss- and gain-of-function studies. Genetics. 2020;214(4):755–767. doi:10.1534/genetics.119.302964.

Editor: E. Gavis